NETZERO 10.66967/netzero.2026.v2i202 CoSci Press

Research Article

Spatiotemporal Coastal Air-Quality Contrasts under Transboundary Influence: Sentinel-5P CO and NO_2 over Prince Edward Island (Canada) and Massachusetts (U.S.)

Andrew d'Entremont [1], Akua Attoh [1], Davoud Ghahremanlou [1,*], Amir Ghahremanlou [2]

[1] Faculty of Business Administration, Memorial University of Newfoundland, St. John's, NL A1B 3X9 Canada.
[2] Department of Civil Engineering, Science and Research Branch, Islamic Azad University, Tehran 1477893855, Iran.
* Corresponding author: dghahremanlo@mun.ca

Article History: Received 3 July 2026; Revised 14 August 2026; Accepted 27 October 2026; Published 29 October 2026

Abstract: Coastal and island airsheds experience compound pressures from local emissions and long-range transport, yet multi-year comparisons between lower-emission island receptors and densely urbanized coastal jurisdictions remain limited. Using Prince Edward Island (PE), Canada, and Massachusetts (MA), U.S., a lower-emission island and a densely urbanized coastal state, we analyse Sentinel-5P TROPOMI observations from 2019 to 2024 to compare column behaviour of CO and NO_2, pollutants with contrasting atmospheric lifetimes. The results show that (1) CO exhibits closely synchronized jurisdiction-scale behaviour consistent with a strong regional-background influence, including elevations in 2023, with closely similar province/state means and overlapping 95% confidence intervals; (2) NO_2 exhibits opposing seasonal regimes, with PE summer-elevated (mean summer ≈ 7.5×10^{-5} mol m^{-2}) and MA winter-elevated (≈4.2×10^{-5} mol m^{-2}), producing a counterintuitive PE > MA annual mean despite higher localized urban peaks in MA; (3) spatial maps show compact corridor-associated NO_2 hotspots in MA versus a comparatively more spatially diffuse NO_2 pattern in PE; and (4) exploratory concordance with independent external evidence shows construct-dependent correspondence across pollutants and jurisdictions. The six-year temporal and spatial patterns support a screening-versus-compliance framework in which satellite columns can help prioritize season-specific ground monitoring, identify candidate corridors for follow-up, and support smoke-event screening, while exposure assessment and regulatory compliance remain based on validated surface observations or appropriately validated fused products. The findings therefore support summer NO_2 monitoring priorities in PE and winter corridor monitoring in MA and provide a transferable screening framework for other coastal and island jurisdictions.

Keywords: Sentinel-5P; spatiotemporal trends; coastal air quality; transboundary pollution; nitrogen dioxide; carbon monoxide; satellite–external evidence concordance; policy implications

1. Introduction

Coastal and island airsheds are shaped by the interaction of local emissions, concentrated human activity, and long-range atmospheric transport. More than 0.6 billion people lived in coastal areas in 2000, and this population is projected to exceed 1.3 billion by 2060 [1]. Transport, industrial activity, and energy-related combustion contribute CO and NO_2, while prevailing winds can redistribute pollutants and their precursors across coastal and downwind regions [2–5]. These characteristics make coastal jurisdictions useful settings for examining how local source intensity and regional transport shape atmospheric column burdens. Sentinel-5P TROPOMI provides spatially consistent, near-daily observations that can complement limited ground monitoring and enable comparative assessment across contrasting coastal environments [5]. More broadly, recent environmental-governance research emphasizes that transboundary environmental risks require integrated monitoring, interoperable evidence streams, and coordinated risk-management frameworks rather than reliance on a single source of information [6].

Within the context of the study regions, Massachusetts faces challenges from significant urban air pollution. A high-resolution multipollutant assessment estimated that on-road emissions contribute approximately 342 premature deaths annually in Greater Boston, with 87% of these deaths linked to elevated NO_2 concentrations [7]. Using a regional Earth system model with TROPOMI constraints, Huang et al. further demonstrated that the northeastern U.S., including Massachusetts, exhibits NO_x-limited or transitional chemical regimes, where NO_2 reductions directly lower surface O_3 concentrations [8]. PE, by contrast, represents a lower-emission island setting with limited ground-monitoring coverage, making broad-area satellite observations particularly useful for jurisdiction-scale assessment. These regional disparities underline the need for localized monitoring, as transboundary pollution from continental sources affects PE's rural airshed, whereas MA's dense traffic and industrial activity contribute to stronger localized NO_2 enhancements. Extensive studies track CO and NO_2 using ground networks and spaceborne sensors. However, jurisdiction-scale diagnosis remains constrained in coastal and island settings due to the limited station density and coarser-resolution products. Sentinel-5P enables consistent, near-daily mapping of CO and NO_2 at high resolution. However, most applications analyse brief intervals, such as lockdown months [9] and wildfire episodes [10,11], and therefore, multi-year, jurisdiction-scale dynamics remain underexplored. Furthermore, existing Sentinel-5P applications are largely single-pollutant, CO [11–14] or NO_2 [15–17], and site-specific like the New York metropolitan area [16], the City of Boston [18], and the Thessaloniki area in Greece [19], limiting generalization beyond individual pollutants/cities. Recent Sentinel-5P studies have demonstrated strong seasonality in NO_2 over major point sources such as thermal power plants, emphasizing the role of meteorology and transport in shaping column patterns [20]. Recent work has begun to extend Sentinel-5P analysis to paired coastal jurisdictions; for example, Lacey et al. examined multi-year CO and NO_2 variability across contrasting North Atlantic and Gulf of Mexico settings [21]. However, an important comparative gap remains in understanding how pollutants with different atmospheric lifetimes behave across a lower-emission island receptor and a densely urbanized coastal state that are both influenced by broadly shared regional

transport. The unresolved question is therefore not whether TROPOMI can characterize CO or NO_2 variability, but how pollutants with contrasting atmospheric lifetimes differ in their temporal coherence, seasonal behaviour, and spatial organization across these two contrasting jurisdictional settings. A side-by-side PE–MA comparison provides an opportunity to examine this question while maintaining a clear distinction among satellite column burden, surface concentration, and emissions. Accordingly, an elevated TROPOMI column is interpreted in this study only as an increased vertically integrated atmospheric burden over the satellite footprint at overpass time. Such an enhancement may reflect stronger local emissions, regional transport, changes in vertical mixing or boundary-layer depth, or a combination of these processes; it is not interpreted as a direct estimate of surface concentration or emission flux. Sentinel-5P is therefore used as a broad-area screening layer, while source attribution, exposure assessment, and regulatory interpretation require independent surface, meteorological, or other supporting evidence.

To address the forementioned literature gaps, this study's primary objective is to integrate high-resolution satellite monitoring of atmospheric pollutants with independent external evidence to assess air quality dynamics across Prince Edward Island (PE), Canada, and Massachusetts (MA), U.S. Using Sentinel-5P satellite data from 2019 to 2024, we primarily focus on CO and NO_2 column density to track pollution levels rather than direct emissions. PE and MA provide a deliberately contrasting coastal pair: PE is a comparatively lower-emission island jurisdiction, whereas MA is a densely populated and urban-industrial coastal state. Both are influenced by prevailing mid-latitude westerlies and regional transport from eastern North America. Their comparison therefore provides a useful setting for examining whether CO and NO_2, which differ substantially in atmospheric lifetime and sensitivity to local versus regional influences, respond differently to the combination of local emissions, spatial averaging, and regional transport. These expectations are grounded in differences in atmospheric lifetime, source geometry, seasonal mixing, and satellite representativeness. CO has a comparatively long atmospheric lifetime and is efficiently transported over regional scales, so jurisdictions influenced by a broadly shared synoptic circulation can exhibit coherent background variability despite substantial differences in local emissions [12,22,23]. In contrast, NO_2 is shorter-lived and more responsive to local combustion sources, seasonal atmospheric mixing, and coastal transport. In urban coastal environments, horizontal advection, boundary-layer evolution, and sea-breeze circulation can strongly modify NO_2 column behaviour and its relationship with surface concentrations [24,25]. Concentrated traffic and combustion sources are also expected to produce sharper spatial NO_2 gradients in densely urbanized areas, whereas more regionally influenced receptor environments can exhibit comparatively diffuse spatial patterns [26–28]. Finally, satellite–surface correspondence depends on spatial heterogeneity, vertical mixing, retrieval resolution, and pollutant lifetime; steep sub-pixel urban gradients can weaken NO_2 correspondence, while the vertically integrated and regionally mixed nature of CO can further decouple total-column variability from surface conditions [12,27]. Based on these physical considerations, we test four a priori hypotheses.

H1: PE and MA will exhibit similar jurisdiction-scale CO columns and broadly synchronous temporal anomalies, consistent with the stronger regional-background influence expected for a relatively long-lived pollutant.

H2: NO_2 will exhibit stronger jurisdiction-specific seasonality than CO because of its shorter lifetime and greater sensitivity to seasonal emissions, atmospheric mixing, and transport, with MA expected to show a pronounced cold-season enhancement relative to its warm season.

H3: MA will exhibit stronger spatial heterogeneity and higher localized NO_2 peaks concentrated along urban and transportation corridors, whereas PE will exhibit a comparatively more spatially diffuse NO_2 pattern.

H4: Annual satellite column variability will show limited and construct-dependent concordance with independent external evidence because atmospheric column burden, reported emissions, and near-surface concentrations represent different physical quantities and spatial domains.

The study makes three specific contributions. First, it extends recent paired coastal Sentinel-5P research by deliberately contrasting a lower-emission island receptor with a densely urbanized coastal state under a broadly shared regional transport regime, thereby isolating a sharper contrast in local source intensity and spatial organization. Second, it uses the contrasting atmospheric lifetimes of CO and NO_2 as an explicit interpretive framework for testing differences in jurisdiction-scale temporal coherence, seasonality, and spatial concentration rather than treating the two pollutants as parallel indicators. Third, it integrates these temporal and spatial contrasts with a construct-aware external-evidence assessment and translates the findings into a screening-to-follow-up framework that distinguishes satellite column burden from emission flux, surface concentration, exposure, and regulatory compliance. The rest of the paper is structured as follows: Section 2 describes the methodology, including the study area (Section 2.1) and the data/processing workflow (Section 2.2). Section 3 presents the results: Sections 3.1 and 3.3 evaluate H1 using annual and monthly jurisdictional means and confidence intervals; Section 3.2 evaluates H2 via multi-year seasonal contrasts; Section 3.4 evaluates H3 using map-based spatial patterns; and Section 3.5 evaluates H4 through exploratory satellite–inventory and satellite–surface concordance with independent external evidence streams. Section 4 interprets the observed temporal and spatial contrasts and discusses plausible mechanisms; Section 4.1 presents evidence-bounded policy implications, and Section 4.2 provides an operational monitoring framework. Section 5 concludes and outlines future directions.

2. Materials and Methods

Sentinel-5P TROPOMI observations were used to characterize carbon monoxide (CO) and nitrogen dioxide (NO_2) column densities over Prince Edward Island (PE) and Massachusetts (MA) from 2019 to 2024. The overall analytical workflow is summarized in Figure 1. Satellite observations were retrieved through Google Earth Engine (GEE), subjected to retrieval-quality, cloud-fraction, solar-zenith-angle, and temporal-completeness screening, and processed to derive area-weighted jurisdictional summaries. The analysis then proceeded through three complementary branches. Temporal analysis evaluated annual, seasonal, and monthly variability and the jurisdiction-scale contrasts addressed by H1 and H2. Spatial analysis used continuous Sentinel-5P fields and Jenks Natural Breaks maps to characterize within-panel spatial organization relevant to H3. The exploratory external-evidence analysis related PE satellite columns to reported emissions inventories and MA satellite columns to ambient surface-monitoring observations to evaluate H4, while recognizing that these comparator streams represent different physical constructs. The combined evidence was interpreted as a screening framework for identifying pollutant-specific temporal patterns, spatially concentrated or diffuse signals, and candidate periods or locations for independent follow-up. Satellite column enhancements were therefore not interpreted as direct measures of local emission flux, surface exposure, or regulatory-standard exceedance.

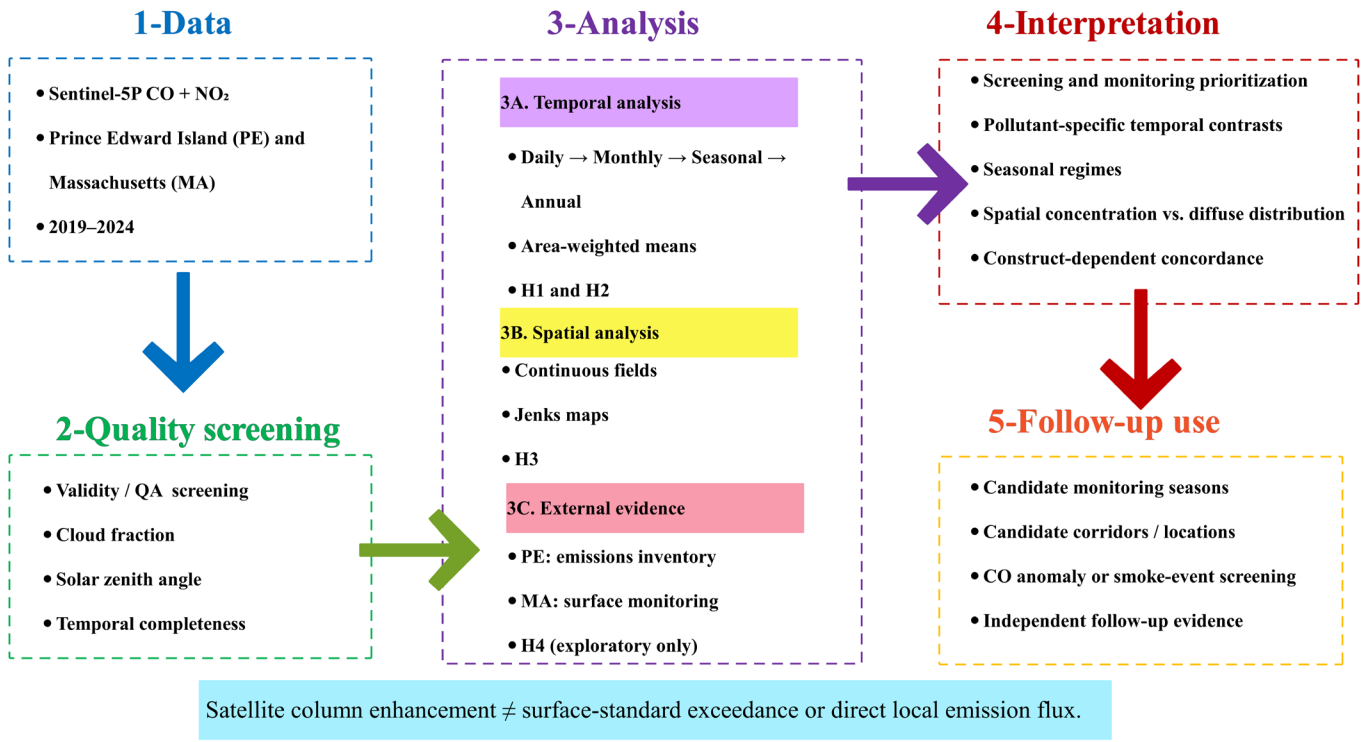


Figure 1. Analytical workflow for the Sentinel-5P assessment over Prince Edward Island (PE) and Massachusetts (MA), 2019–2024. Following data acquisition and quality screening, the analysis was organized into three complementary branches: (A) temporal analysis of daily, monthly, seasonal, and annual jurisdictional summaries supporting H1 and H2; (B) spatial analysis of continuous fields and Jenks-classified maps supporting H3; and (C) exploratory comparison with independent external evidence, reported emissions inventories in PE and ambient surface-monitoring observations in MA, supporting H4. Outputs were integrated for screening-oriented scientific interpretation and identification of candidate monitoring periods and locations requiring independent follow-up. Satellite column enhancement does not by itself indicate surface-standard exceedance or direct local emission flux.

2.1. Study Area

Prince Edward Island (PE: ~6,023 km^2 , ~180,000 population in 2024) in Canada (Figure 2b) [29] is located north of Massachusetts (MA: ~27,335 km^2, ~7.1 million residents in 2024) in the U.S. (Figure 2c); both are coastal, hosting sensitive coastal ecosystems, separated by less than 500 miles across the Gulf of Maine in the North Atlantic (Figure 2a) [30]. As Canada's smallest province, PE's economy is primarily based on agriculture and tourism, with comparatively limited local combustion sources. Thus, it can serve as a background receptor, where a substantial share of observed pollution reflects synoptic transport from upwind continental sources rather than purely local emissions. In contrast, MA is highly industrialized, with the Boston metropolitan area and a dense network of highways and industries. This region has strong internal (point-source) pollution sources (e.g., traffic, power plants, and industrial facilities), which led to an estimated 2,780 deaths during 2019 [31]. Both regions are situated under the prevailing westerlies, and they frequently receive air masses transported from continental source regions (e.g., the U.S.-Canada industrial belt), enabling focused study of transboundary pollution [32,33]. Thus, monitoring pollutants such as NO_2 (a precursor to acid rain) and CO (which affects both air quality and human health) is of critical importance for understanding the pressures exerted on these environments.

2.2. Data Compilation Methods

We extracted CO and NO_2 column number densities from Sentinel-5P COPERNICUS/S5P/NRTI/L3_CO and L3_NO_2 for 2019–2024 and clipped the observations to PE and MA. Quality screening followed the Sentinel-5P product documentation and the validity filtering applied during conversion of the Level-2 products to the Google Earth Engine Level-3 collections. Additional screening was applied using a cloud-fraction criterion of <0.60 and a solar-zenith-angle criterion of ≤70° to reduce heavily cloud-contaminated and high-angle observations while preserving adequate temporal sampling in the coastal study domains. The 0.50 NO_2 quality level is a documented permissive threshold that retains additional valid retrievals under cloudy or snow/ice conditions, whereas more restrictive screening is recommended for many tropospheric-NO_2 applications [34] Daily retrievals were retained at native resolution, and duplicate overpasses within a day were averaged. Monthly means were calculated from valid daily observations only and were retained when at least 10 valid observation days were available within the month. This minimum-completeness criterion was imposed to prevent monthly estimates from being determined by only a few isolated satellite overpasses. Seasons were defined meteorologically as winter (December–February; DJF), spring (March–May; MAM), summer (June–August; JJA), and fall (September–November; SON). Annual means were retained when at least eight monthly means satisfied the monthly completeness criterion, thereby excluding years with severely sparse temporal coverage. These thresholds were treated as data-completeness gates rather than guarantees of unbiased temporal sampling; no missing days or months were imputed. A targeted sensitivity assessment was additionally conducted to evaluate the effect of applying a more restrictive NO_2 quality threshold of 0.75 instead of the permissive 0.50 threshold, while retaining the same cloud-fraction, solar-zenith-angle, daily-aggregation, and temporal-completeness criteria. The assessment focused particularly on cold-season retrieval availability and on whether the principal jurisdiction-specific seasonal interpretation was preserved under

the more restrictive screening. Under the baseline screening, a completeness audit confirmed that all monthly values entering the seasonal analyses met the ≥10-valid-day criterion, with no season systematically absent from the PE record. Because cloud screening can produce non-random temporal sampling, particularly in maritime environments, persistent seasonal cloudiness may still preferentially remove particular meteorological conditions even when these completeness criteria are satisfied. Satellite NO_2 studies have shown that cloud-based observation selection can bias longer-term averages when cloudy and clear conditions correspond to systematically different pollution regimes [35]. We therefore interpret the seasonal and annual summaries as quality-screened satellite climatologies of the available retrievals and consider possible cloud-related seasonal sampling bias when interpreting the PE–MA contrasts. Jurisdictional summaries were calculated as area-weighted pixel means. Column anomalies were therefore interpreted as changes in vertically integrated atmospheric burden; attribution to local emissions, regional transport, or vertical mixing was treated as mechanistic interpretation unless independently supported. Because annual and seasonal jurisdictional values were naturally paired by calendar year and only six yearly pairs were available, key a priori PE–MA and within-jurisdiction seasonal contrasts were evaluated using two-sided exact paired randomization tests based on all 2^6 sign permutations of the paired differences. Exact p-values are reported alongside descriptive means and confidence intervals. The exploratory four- and five-point concordance regressions were not subjected to inferential significance testing because of their very small sample sizes and construct-specific purpose.

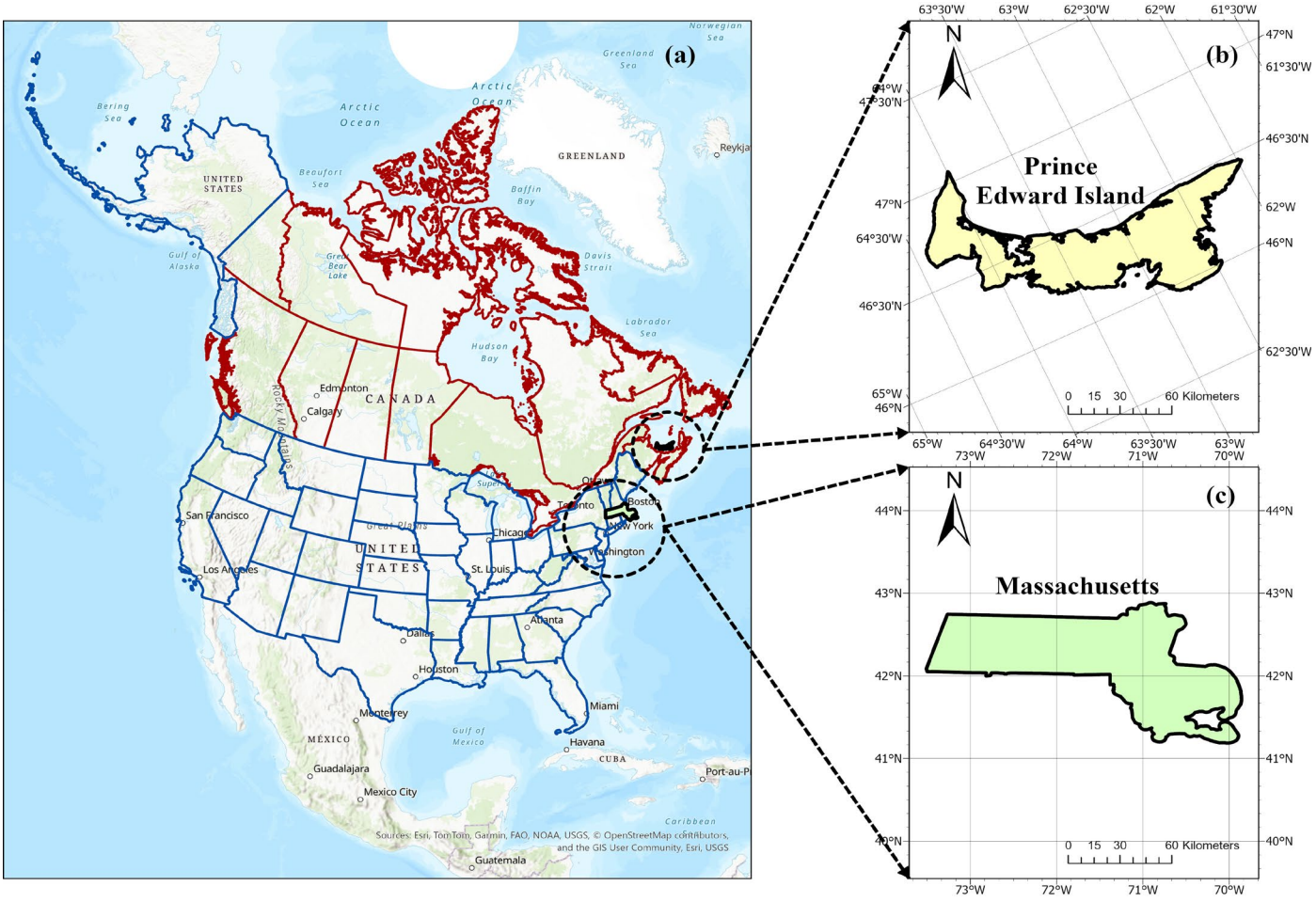


Figure 2. The study area's geographic position (**a**) globally, (**b**) Prince Edward Island, (**c**) Massachusetts

External-data availability was asymmetric across jurisdictions and pollutants. PE provides a jurisdiction-wide annual emissions inventory for both CO and NO_x, whereas a comparable continuous surface-monitoring series covering both pollutants was not available for the provincial network used in this study [36]. MA, in contrast, provides annual ambient monitoring observations for both CO and NO_2 over the study period, whereas an equivalent annual state-level emissions series with the same pollutant and temporal coverage was not available for the present analysis [37]. We therefore selected one internally consistent external-evidence stream for both pollutants within each jurisdiction, reported emissions inventories in PE and ambient surface concentrations in MA, rather than mixing comparator types within a jurisdiction. The resulting comparator quantities represent different physical constructs. For PE, the analysis relates Sentinel-5P atmospheric column burden to jurisdiction-level reported emission flux, whereas for MA it relates satellite column burden to near-surface ambient concentration. No conversion among column density, emission flux, and surface concentration was attempted because such harmonization would require additional assumptions regarding atmospheric transport, mixing, chemistry, and vertical structure, following the screening logic used by Ghahremanlou and Ghahremanlou [38]. Accordingly, the four concordance relationships were interpreted separately as exploratory evidence streams and were not used to compare concordance strength or satellite performance directly between PE and MA. A bounded 2020–2023 interval was retained for this exploratory concordance analysis to maintain methodological consistency with the previously published satellite–inventory screening framework of Ghahremanlou and Ghahremanlou [38]. This four-year interval was used only for the external-evidence concordance assessment; the primary Sentinel-5P temporal,

seasonal, and spatial analyses retained the full 2019–2024 record. The concordance analysis was therefore not intended to estimate long-term trends or to assess COVID-19-related changes. With only four annual paired observations for each pollutant–jurisdiction relationship, the resulting regression statistics were interpreted descriptively and not as robust estimates of predictive performance, causal relationships, regulatory thresholds, or evidence of equivalence among column burden, reported emissions, and surface concentration. As a sensitivity check, the concordance analysis was additionally repeated over 2019–2023 where corresponding annual external data were available. This five-year analysis was used only to determine whether inclusion of the pre-2020 observation materially altered the qualitative concordance interpretation.

Maps were classified using the Jenks Natural Breaks algorithm with five classes and 1,000 iterations. The method identifies natural groupings by minimizing within-class variation and maximizing separation among classes. Five classes were selected a priori to provide an interpretable sequence of Very Low, Low, Moderate, High, and Very High categories while retaining sufficient spatial detail for visualization. Jenks breaks were calculated independently for each pollutant–jurisdiction–year panel. Consequently, the class labels represent relative within-panel categories and are not quantitatively comparable across years or jurisdictions. The maps were therefore used to identify the location and spatial concentration of relatively elevated or reduced values within each panel, whereas temporal and jurisdictional comparisons were based on the underlying continuous column values and the annual, seasonal, and monthly summaries [39].

3. Results

3.1. Annual Temporal Trends

Mean annual satellite-based CO and NO_2 columns over 2019–2024 are summarized in Figure 3, with complete numerical values and summary statistics provided in Table S3. CO showed closely similar interannual behaviour in PE and MA, declining in both jurisdictions in 2022 and reaching relatively high values in 2021 and 2023. Across the six paired years, the jurisdictional CO means were closely similar (PE: 0.0346 mol m^{-2}; MA: 0.0348 mol m^{-2}), with similar interannual standard deviations (0.00155 and 0.00154 mol m^{-2}, respectively). The paired annual CO difference did not reach the 0.05 level under the exact randomization test ($p = 0.063$). In contrast, annual NO_2 columns were higher in PE in all six years, ranging from 5.66×10^{-5} to 6.14×10^{-5} mol m^{-2} in PE compared with 3.37×10^{-5} to 3.82×10^{-5} mol m^{-2} in MA. The six-year means were 5.94×10^{-5} mol m^{-2} for PE and 3.54×10^{-5} mol m^{-2} for MA, and the paired annual difference was supported by the exact randomization test ($p = 0.031$).

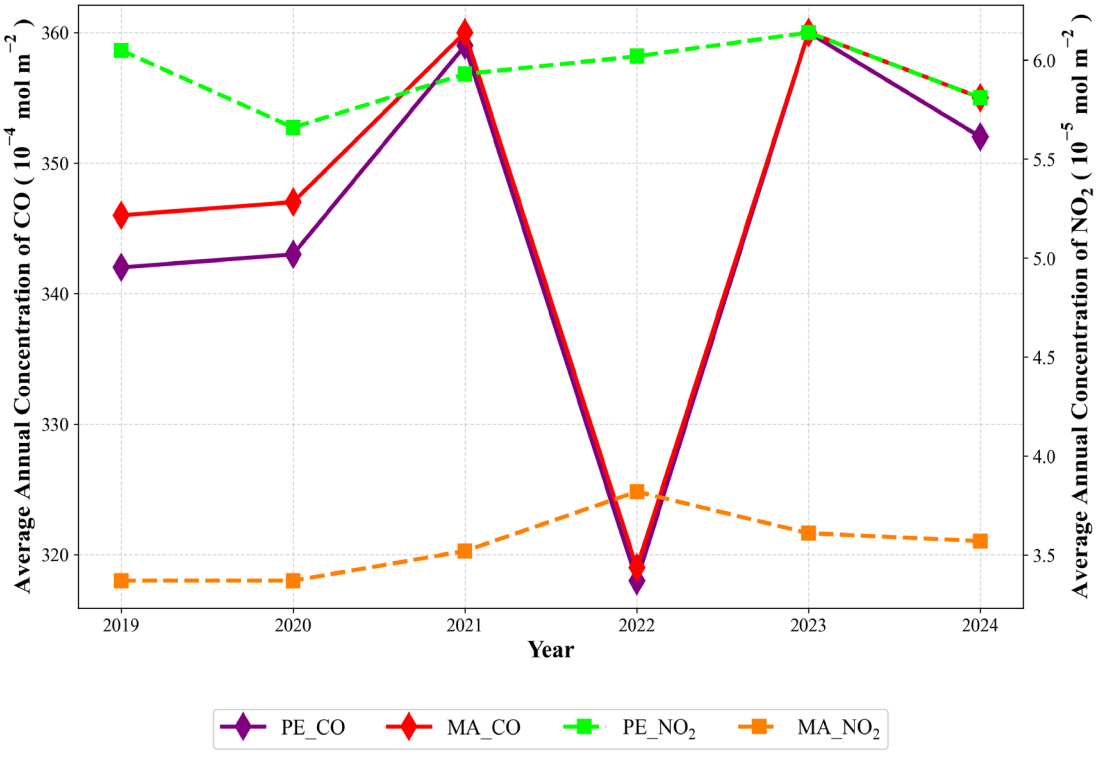


Figure 3. Annual mean Sentinel-5P column densities of CO and NO_2 over Prince Edward Island (PE) and Massachusetts (MA) from 2019 to 2024. CO is shown on the left axis and NO_2 on the right axis. Complete annual values and summary statistics are provided in Table S3.

3.2. Seasonal Patterns

Seasonal patterns shown in Figure 4, with complete numerical values and summary statistics provided in Table S4, indicate that CO exhibits similar warm-season behaviour in both PE and MA, with spring and summer means (PE: ≈0.0367 mol m^{-2} > 0.0355 mol m^{-2}; MA: ≈0.0373 mol m^{-2} > 0.0360 mol m^{-2}) consistently higher than fall means (PE: ≈0.0331 mol m^{-2} and MA: ≈0.0328 mol m^{-2}), confirming robust warm-season enhancements and fall minima. Interannual variability is season-dependent: winter shows the smallest spread (STDEV: PE ≈ 0.00128 mol m^{-2}, MA ≈ 0.00131 mol m^{-2}), whereas summer is largest (PE: ≈0.00407 mol m^{-2}, MA: ≈0.00393 mol m^{-2}) in both regions. Seasonal CO means and their 95% confidence intervals were closely similar between PE and MA, indicating broadly comparable seasonal behaviour at the jurisdiction scale. Within each jurisdiction, spring and summer intervals generally sit above fall, reinforcing the robust warm-season enhancement and fall minima reported above.

NO_2 exhibited distinct seasonal regimes in the two jurisdictions. In PE, the summer mean was approximately 7.5×10^{-5} mol m^{-2} compared with 3.9×10^{-5} mol m^{-2} in winter, and the

summer–winter difference was supported by the exact paired randomization test (p = 0.031). MA exhibited the opposite pattern, with winter NO_2 averaging approximately 4.2 × 10^{-5} mol m^{-2} compared with 2.7 × 10^{-5} mol m^{-2} in summer (p = 0.031). Between jurisdictions, the PE–MA NO_2 difference was supported in spring, summer, and fall (p = 0.031 for each), whereas the winter difference was not supported at the 0.05 level (p = 0.313). These formal tests support the opposing jurisdiction-specific seasonal regimes identified in H2. Increasing the NO_2 quality threshold from 0.50 to 0.75 did not alter the principal seasonal interpretation. For PE, matched seasonal means changed by only −1.76% in winter, −0.45% in spring, +1.00% in summer, and −1.50% in fall, while the pronounced summer-over-winter contrast was preserved. Retrieval availability was most sensitive during winter; the only month falling below the ≥10-valid-day completeness criterion under the more restrictive screening was January 2022 in PE, which retained 9 valid days compared with 24 days under the baseline screening. The overall jurisdiction-specific seasonal interpretation therefore remained unchanged, with PE characterized by a summer maximum and MA by a winter maximum. These results support the robustness of the opposing seasonal regimes identified in H2 while indicating greater retrieval sensitivity during the cold season.

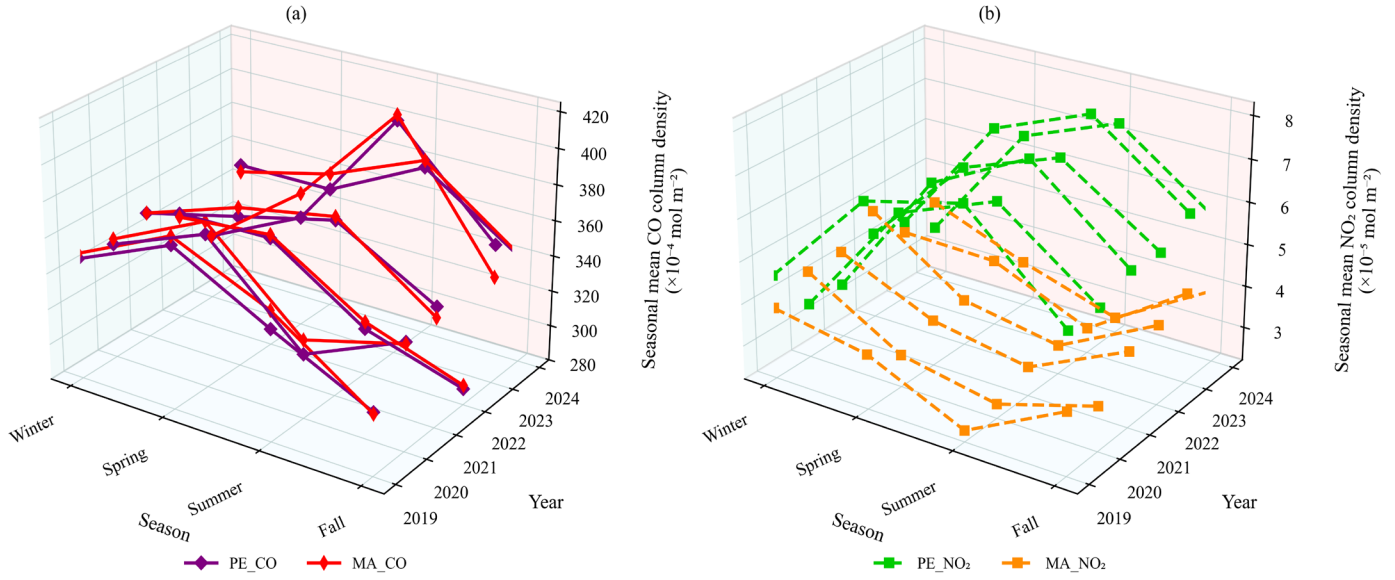


Figure 4. Seasonal Sentinel-5P column densities of (**a**) CO and (**b**) NO_2 over Prince Edward Island (PE) and Massachusetts (MA) from 2019 to 2024. The x-axis represents meteorological season, the y-axis represents year, and the z-axis shows the corresponding seasonal mean column density. Solid lines denote CO (PE: purple; MA: red), whereas dashed lines denote NO_2 (PE: green; MA: orange). Each year is represented by a separate seasonal trajectory, allowing interannual and jurisdiction-specific seasonal patterns to be compared simultaneously. Complete numerical values and summary statistics are provided in Table S4.

3.3. Monthly Trends

Monthly Sentinel-5P CO and NO_2 time series are shown in Figure 5, with complete monthly values provided in Table S1 and month-specific summary statistics in Table S2. For CO, the monthly time series confirms recurring summertime peaks and fall minima shown in Figure 4 and highlights extreme monthly values such as the high of 0.0419 mol m^{-2} in August 2023 over PE and 0.0431 mol m^{-2} in July 2021 over MA, and the lowest values in October 2022 (PE: 0.0286 and MA: 0.0279 mol m^{-2}). Likewise, Table S1 shows strong month-to-month structure for NO_2, with PE reaching a maximum of ≈8.2 × 10^{-5} mol m^{-2} in July 2023 and a minimum of ≈2.6 × 10^{-5} mol m^{-2} in December 2023, while MA peaks later in the year (≈5.8 × 10^{-5} mol m^{-2} in November 2023) and reaches its lowest value in August 2023 (≈2.2 × 10^{-5} mol m^{-2}). The monthly statistical summary in Table S2 shows interannual variability in the column burden for each month. For CO, variability is smallest in late fall-winter and largest in mid-summer (July–August STDEV ≈ 0.004–0.005 mol m^{-2} in both jurisdictions), and PE–MA 95% CIs overlap for every month (e.g., July: PE 0.0313–0.0413 vs. MA 0.0313–0.0424 mol m^{-2}; January: PE 0.0327–0.0353 vs. MA 0.0328–0.0352 mol m^{-2}), indicating no statistically discernible between-jurisdiction difference in monthly CO means. For NO_2, monthly structure is strongly separated outside winter: spring, summer, and early-fall CIs do not overlap with PE > MA (e.g., July: PE 7.3 × 10^{-5}–7.9 × 10^{-5} vs. MA 2.5 × 10^{-5}–2.9 × 10^{-5} mol m^{-2}; September: PE 6.1 × 10^{-5}–6.9 × 10^{-5} vs. MA 2.6 × 10^{-5}–3.0 × 10^{-5} mol m^{-2}), whereas winter months show overlapping CIs (e.g., January: PE 2.8 × 10^{-5}–4.2 × 10^{-5} vs. MA 3.5 × 10^{-5}–5.3 × 10^{-5} mol m^{-2}), consistent with the opposing seasonal regimes already established and revealing which months drive the divergence.

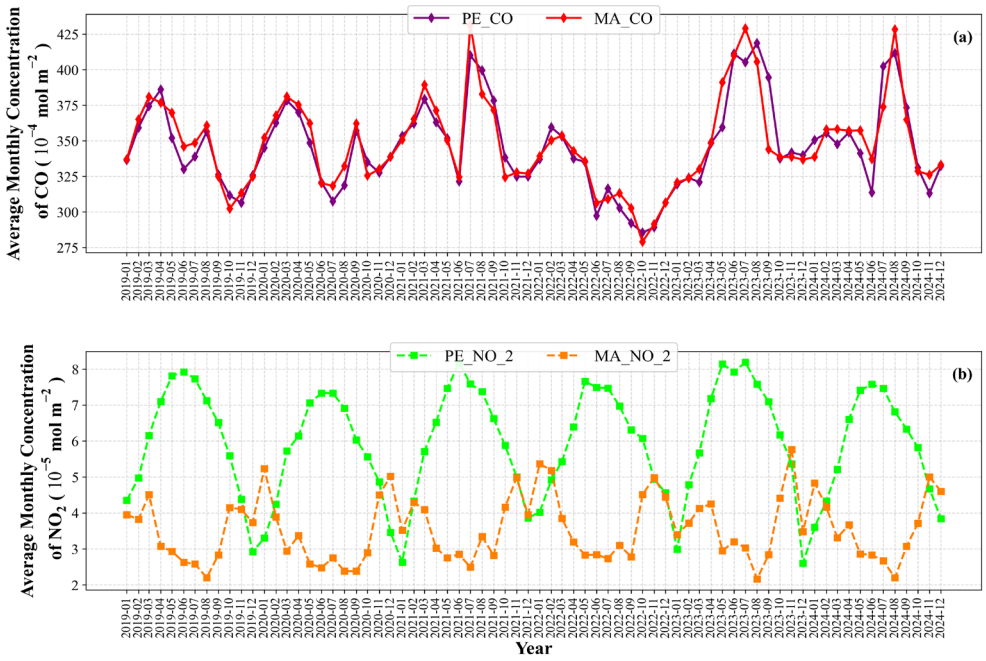


Figure 5. Monthly mean Sentinel-5P column densities of (**a**) CO and (**b**) NO_2 over Prince Edward Island (PE) and Massachusetts (MA) from January 2019 to December 2024. Purple and red lines denote PE and MA CO, respectively; green and orange lines denote PE and MA NO_2, respectively. Complete monthly values and summary statistics are provided in Tables S1 and S2.

3.4. Spatial Changes of Pollutants

Figure 6 shows spatial variability in CO across PE and MA from 2019 to 2024. In PE, relatively elevated within-panel values are repeatedly located near populated areas including Summerside and parts of western PE, while much of the island exhibits lower values within each annual map. In MA, spatial heterogeneity is stronger, with recurrent local maxima centered on the Greater Boston urban region and other major populated corridors. Because Jenks breaks were calculated independently for each panel, the class labels are interpreted only relative to the distribution within each individual map; apparent changes in the spatial extent of named classes are therefore not used to infer quantitative expansion or contraction across years or jurisdictions.

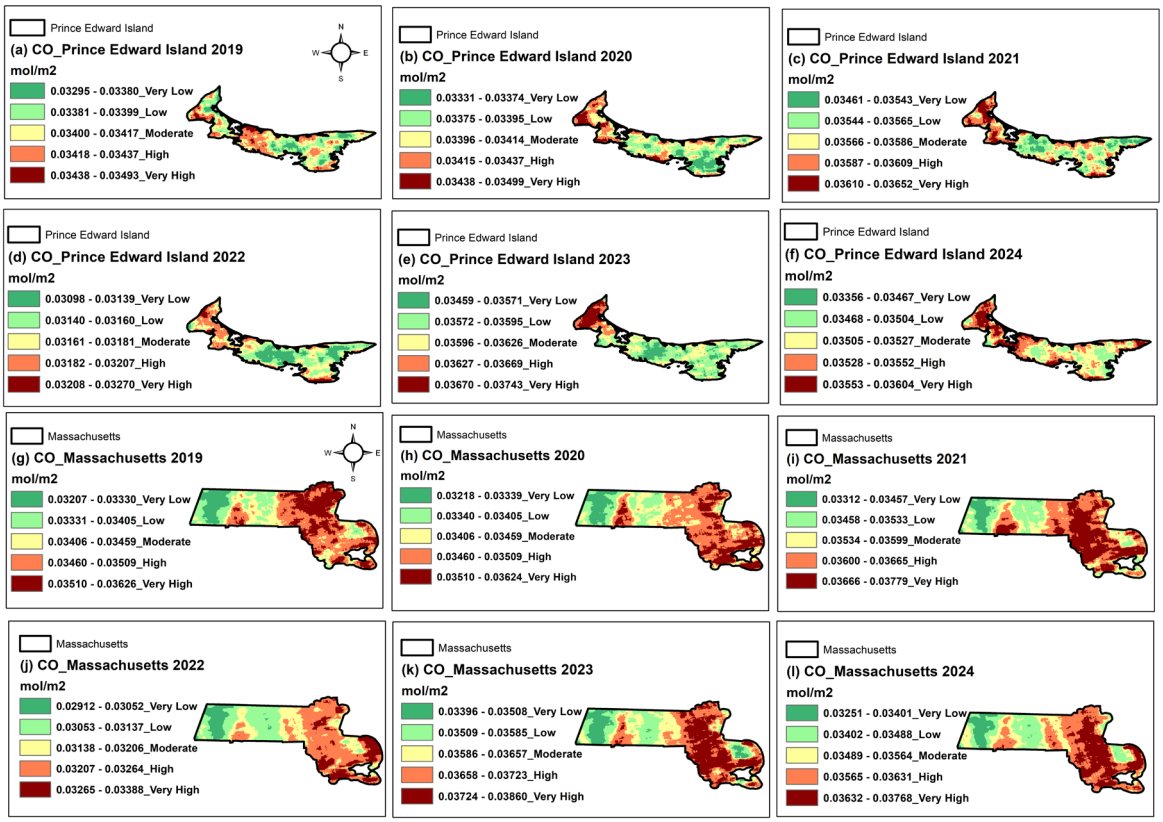


Figure 6. Spatial distribution of CO over Prince Edward Island (**a**–**f**) and Massachusetts (**g**–**l**) from 2019 to 2024. Jenks Natural Breaks were calculated independently for each panel; therefore, class colours represent relative within-panel categories and should not be interpreted as directly comparable across years or jurisdictions.

Figure 7 shows persistent but spatially varying NO_2 patterns across PE and MA from 2019 to 2024. In PE, relatively elevated within-panel values occur in different parts of the island across years, including western PE in some years and the Charlottetown area in others, indicating a comparatively diffuse and geographically shifting pattern. In MA, the strongest localized values are consistently concentrated in the Greater Boston metropolitan region and northeastern coastal corridor, with secondary elevated areas around Springfield–Worcester and the central Massachusetts corridor. Because Jenks breaks were calculated independently for each panel, differences in the areal extent of class labels such as High or Very High cannot be interpreted quantitatively across years or jurisdictions. The maps are therefore used to identify the location and relative spatial concentration of within-panel maxima, while temporal changes are evaluated from the continuous annual, seasonal, and monthly summaries. Accordingly, H3 is interpreted qualitatively from the persistence, location, and spatial concentration of within-panel maxima rather than from direct comparison of Jenks class thresholds or class areas across panels.

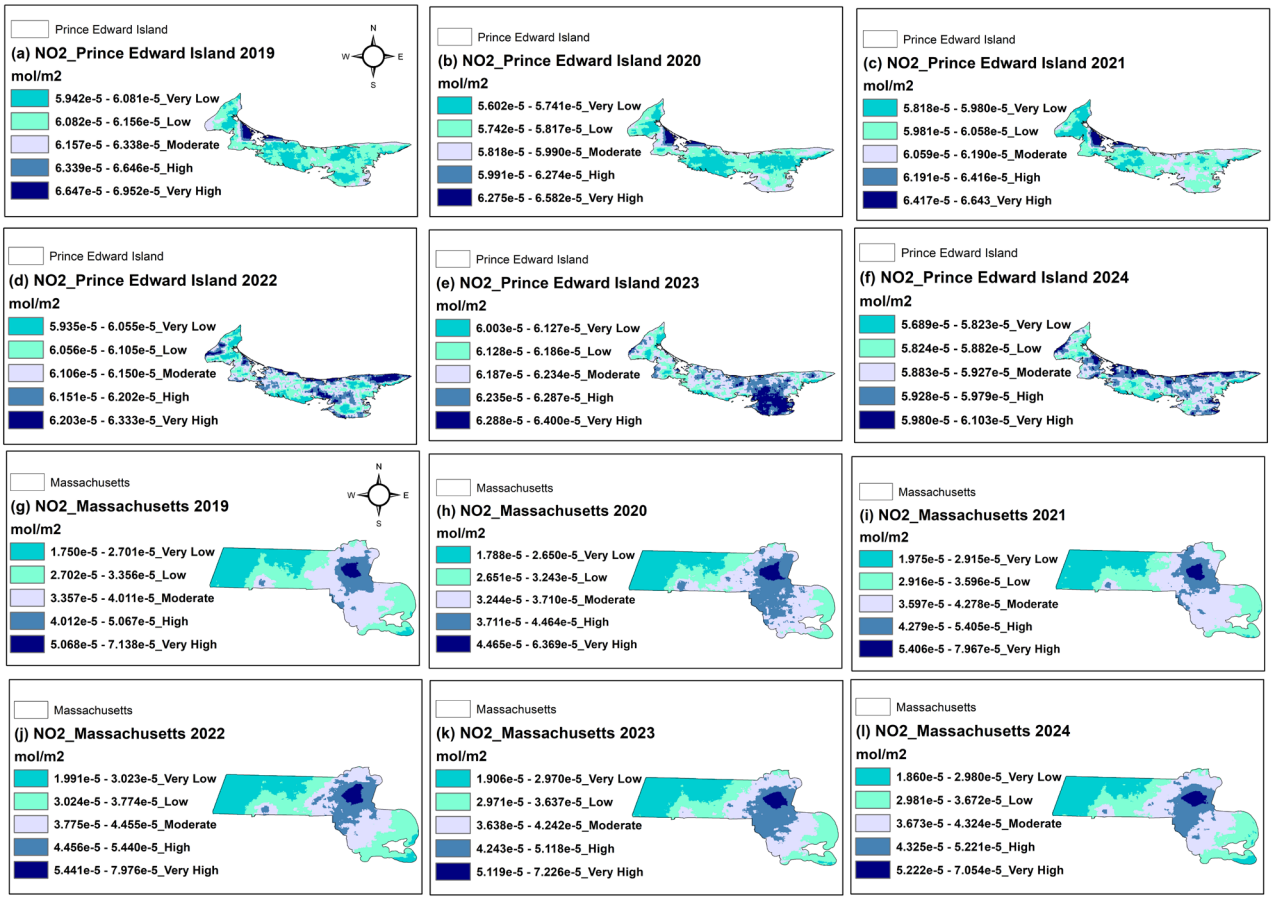


Figure 7. Spatial distribution of NO_2 over Prince Edward Island (**a**–**f**) and Massachusetts (**g**–**l**) from 2019 to 2024. Jenks Natural Breaks were calculated independently for each panel; therefore, class colours represent relative within-panel categories and should not be interpreted as directly comparable across years or jurisdictions.

3.5. Exploratory Satellite–Inventory and Satellite–Surface Concordance

An exploratory concordance analysis was conducted over the bounded 2020–2023 comparison window (Figure 8), separately from the full 2019–2024 satellite record. For PE, annual Sentinel-5P columns were compared with reported emissions inventories, whereas for MA they were compared with ambient surface-monitoring concentrations. Because these comparator streams represent different physical quantities, the relationships were interpreted separately. For PE, satellite–inventory concordance was weak for CO ($R^2 \approx 0.02$) and modest for NO_2 ($R^2 \approx 0.37$). For MA, satellite–surface concordance was weak for both CO ($R^2 \approx 0.00$) and NO_2 ($R^2 \approx 0.02$). With only four annual paired observations per relationship, these values are treated as descriptive consistency indicators rather than robust estimates of predictive performance, statistical thresholds, direct validation, or regulatory suitability. In particular, the PE and MA R^2 values are not interpreted as measures of relative satellite performance because the underlying comparator variables represent different physical constructs. Figure 8 therefore serves only as an exploratory cross-evidence consistency check complementing the denser seasonal, monthly, and spatial analyses presented in Sections 3.1–3.4. The limited and construct-dependent concordance reinforces the use of Sentinel-5P as a broad-area screening layer while reserving exposure and compliance assessment for validated surface observations or appropriately validated fused products.

As for sensitivity, including 2019 as a fifth annual observation did not materially alter these qualitative concordance interpretations. For PE, the CO relationship decreased from $R^2 = 0.023$ over 2020–2023 to $R^2 < 0.001$ over 2019–2023, remaining very weak, while the NO_2 relationship changed from $R^2 = 0.366$ to $R^2 = 0.297$ and remained modest and descriptive. For MA, CO was essentially unchanged ($R^2 = 0.004$ for both periods), whereas NO_2 increased from $R^2 = 0.023$ to $R^2 = 0.106$ but remained weak. Thus, inclusion of the pre-2020 observation did not change the construct-dependent and exploratory interpretation of any of the four concordance relationships.

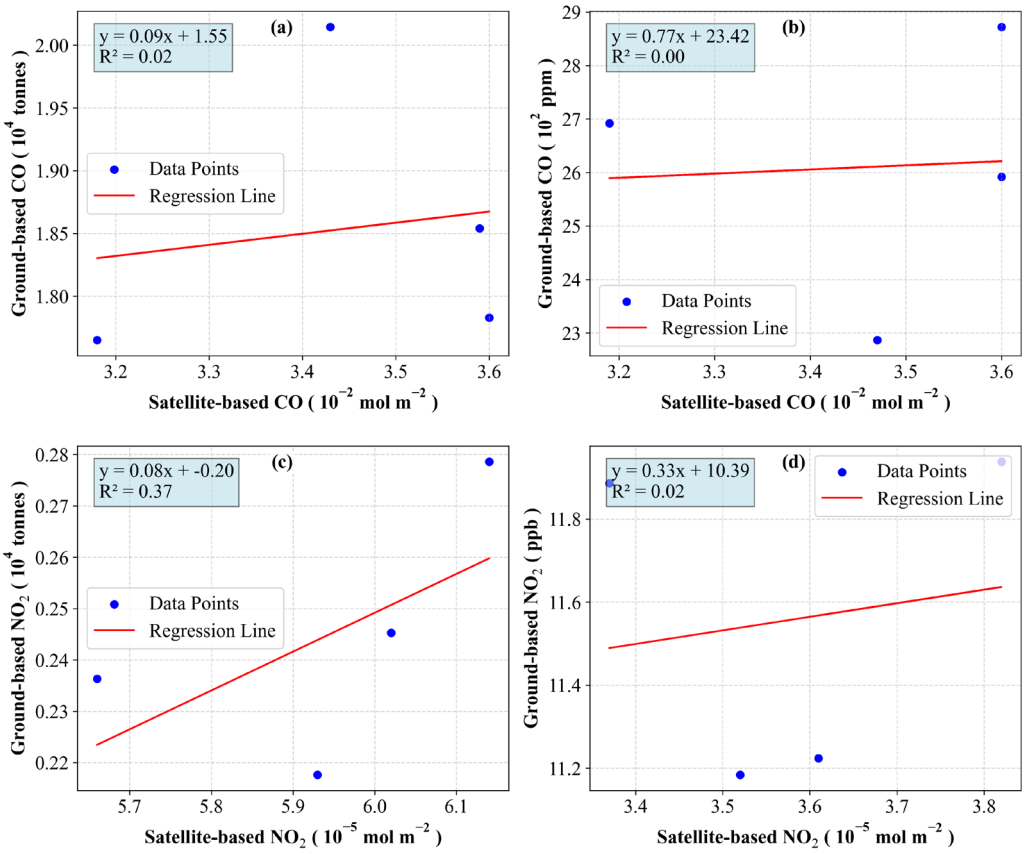


Figure 8. Exploratory concordance between annual Sentinel-5P column densities and independent external evidence during 2020–2023: (**a**) PE CO, reported emissions inventory, (**b**) MA CO, surface concentration, (**c**) PE NO_2, reported emissions inventory, and (**d**) MA NO_2, surface concentration. PE and MA regressions represent different physical constructs and are interpreted separately; R^2 values are descriptive only and do not constitute formal validation or regulatory performance thresholds.

4. Discussion

The central result is a clear pollutant-specific contrast between the two coastal jurisdictions. CO exhibits closely synchronized jurisdiction-scale behaviour, whereas NO_2 shows markedly different seasonal and spatial regimes, including the counterintuitive higher PE jurisdictional mean despite stronger localized urban peaks in MA. Rather than repeating the numerical results reported in Section 3, the Discussion focuses on how pollutant lifetime, spatial averaging, and plausible meteorological and transport processes may contribute to these contrasting patterns, while distinguishing directly observed evidence from mechanisms that require independent verification.

The opposing NO_2 seasonal regimes suggest different combinations of controlling processes in the two jurisdictions. In MA, the winter maximum is consistent with shallower and more stable boundary layers, reduced ventilation, a longer cold-season NO_2 lifetime, and sustained traffic and heating-related NO_x emissions, all of which can favour greater lower-tropospheric NO_2 burdens. Recent TROPOMI evidence likewise shows higher winter and lower summer urban NO_2 at middle and high latitudes, with longer wintertime NO_2 lifetimes and seasonal differences in emissions contributing to this cycle [40]. In dense MA source regions, rapid conversion of freshly emitted NO to NO_2 through reaction with O_3 and seasonally varying reactive-nitrogen and aerosol chemistry may additionally modify wintertime partitioning, although these processes cannot be isolated with the present observational design. In PE, by contrast, the warm-season maximum cannot be explained by NO_2 lifetime alone because stronger summer photochemistry generally shortens NO_2 lifetime. The observed enhancement therefore points to additional warm-season source and transport influences, potentially including soil or agricultural NO_x emissions, episodic biomass-burning influence, and coastal or synoptic redistribution [25]. Recent work over the northeastern and mid-Atlantic United States shows that warm-season soil NO emissions can contribute appreciably to reactive-nitrogen variability and can help explain enhanced warm-season surface and column NO_2 over rural and agricultural regions [28]. Coastal boundary-layer evolution and land–sea circulation may further redistribute NO_2 vertically and horizontally, altering the relationship between satellite columns and near-surface concentrations [24,41]. These mechanisms remain hypotheses rather than source attribution: they predict that PE warm-season enhancements should strengthen during periods favourable to agricultural, fire, or transported influences, whereas MA winter maxima should preferentially coincide with shallow boundary layers, weak ventilation, and elevated combustion activity.

The seasonal evidence in Figure 4 further distinguishes the behaviour of the two pollutants. CO exhibits broadly similar seasonality across PE and MA, consistent with the stronger regional integration expected for a relatively long-lived species [11,22]. NO_2, by contrast, exhibits opposing seasonal regimes, with warm-season enhancement in PE and cold-season enhancement in MA, consistent with the greater sensitivity of short-lived NO_2 to seasonal emissions, atmospheric mixing, and coastal transport [25,42,43]. Importantly, the seasonal pattern held when the NO_2 quality threshold was raised from 0.50 to 0.75: PE seasonal means shifted only slightly, and the summer-over-winter ordering was unchanged. Winter retrievals were more sensitive to the stricter filter, so absolute cold-season NO_2 values warrant more caution than the direction of the seasonal contrast. The monthly analysis shows that this divergence is concentrated in particular parts of the year rather than representing a uniform

year-round jurisdictional difference [10,11,44,45]. Potential contributions from boundary-layer variability, synoptic inflow, and spatial averaging are physically plausible, but their relative importance cannot be resolved from the present observational design [46,47].

For CO (Figure 6), most of PE remains in Low-Moderate classes, with recurring High-Very High patches along the Charlottetown-Stratford-Cornwall urban cluster and the Summerside-Kensington corridor, and with higher-class categories present toward West Prince (e.g., Miminegash–Tignish–Alberton) during fire-affected years (2021/2023). In MA, CO hotspots align with the Greater Boston conurbation, the I-93/I-95 ring (Somerville-Everett-Chelsea), South Shore to Quincy, and Worcester, with the Very High category also present within the 2021 and 2023 panels, coincident with regional wildfire-affected years, but not identified within the 2022 panel. This pattern is consistent with city-scale CO maps from TROPOMI/MOPITT showing intense but spatially compact urban peaks embedded in a broad regional background [11,22,48] and with North American studies reporting fire-year expansions of High/Very High CO classes across large areas [11,49,50]. The apparent combination of strong Boston-centered maxima and similar province/state CO means is therefore consistent with a spatial-averaging effect in which compact peak intensity and broader areal persistence contribute differently to jurisdiction-wide averages [51,52]. This interpretation remains qualitative because source contribution and transport were not independently resolved.

For NO_2 (Figure 7), MA shows a compact, persistent hotspot anchored on the Boston core (Logan/port-Chelsea-Everett-Somerville), with secondary High ribbons along I-90 (Worcester-Springfield) and the Merrimack Valley (Lawrence-Lowell). This spatial concentration over dense transport/heating corridors is consistent with urban NO_2 literature for U.S. metros [16] and similar findings reported globally [53]. In PE, by contrast, elevated classes are distributed across a larger portion of the island within each panel and shift location by year: West Prince in 2019–2021 (e.g., Birch Hill/Miminegash), a marked Central-East emphasis in 2023 (the Charlottetown basin and inland to Peakes), and a more even island-wide distribution in 2024, a pattern consistent with coastal stability and synoptic inflow broadening warm-season NO_2 burdens [23,54–56]. When aggregated, the higher jurisdiction-scale NO_2 mean in PE relative to MA, despite MA's stronger localized peaks (Figure 3, Table S3), is consistent with a spatial-averaging effect based on the underlying continuous Sentinel-5P column values rather than on the Jenks-classified maps, which are used here only to visualize within-panel spatial location and are not compared quantitatively across panels. The proposed roles of boundary-layer structure and regional transport remain physically plausible but unverified in the absence of dedicated meteorological or trajectory analyses [16,23,57].

Within the exploratory 2020–2023 comparison window, CO shows very weak descriptive correspondence with independent external evidence streams in PE ($R^2 \approx 0.02$) and MA ($R^2 \approx 0.00$), while the NO_2 R^2 is higher in PE (≈0.37) than in MA (≈0.02). However, each regression contains only four annual paired observations; consequently, the difference between these R^2 values is interpreted descriptively and is not used to establish a performance threshold, predictive relationship, or differential regulatory applicability between PE and MA. Column–surface correspondence can be affected by representativeness error, temporal mismatch between satellite overpass and surface averaging, vertical mixing, and steep sub-pixel urban gradients [24,26,27]. Accordingly, Figure 8 is treated only as an exploratory consistency check. The policy relevance of the satellite analysis instead derives primarily from the 2019–2024 seasonal, monthly, and spatial evidence, which can identify candidate monitoring periods, persistent high-burden areas, and episodic smoke anomalies. Exposure assessment, source attribution, and regulatory compliance require ground-based observations or separately validated fused products.

This asymmetry reflects data availability rather than an analytical choice: a jurisdiction-wide emissions inventory was available for PE but not a comparable pollutant-matched surface series, and the reverse was true for MA. The apparently higher descriptive NO_2 concordance in PE than in MA should not be interpreted as evidence of superior satellite performance because the comparator constructs differ. Within those distinct constructs, spatial support provides one plausible explanation for the contrast: the PE emissions inventory is aggregated at the jurisdiction scale and may therefore covary more coherently with a jurisdiction-mean satellite column, whereas the MA surface monitors sample localized near-surface conditions within a spatially heterogeneous urban environment. Steep sub-pixel gradients around Greater Boston, variability in vertical mixing, and temporal mismatch between the satellite overpass and surface-monitoring averages can consequently weaken column–surface correspondence. This interpretation is consistent with H4 but cannot be quantitatively separated from the difference in comparator type with the present data.

The present study distinguishes observed evidence from mechanistic interpretation. The temporal and spatial contrasts reported in Tables S1–S4, and Figures 3–7 are directly derived from the Sentinel-5P observations, whereas the proposed roles of boundary-layer dynamics, synoptic transport, and coastal meteorology are literature-supported hypotheses offered to interpret those patterns. Confirming their relative contributions would require independent diagnostics such as ERA5 or comparable reanalysis of boundary-layer height and winds, backward-trajectory analysis, and chemical-transport modelling. These analyses are beyond the scope of the present study and are identified as priorities for future work.

4.1. Policy Implications

The policy implications are deliberately restricted to monitoring priorities supported directly by the observed temporal and spatial patterns. Sentinel-5P columns should be treated as screening evidence in both PE and MA rather than as measures of surface exposure, local emission flux, or regulatory compliance. In PE, the persistent warm-season NO_2 enhancement supports prioritizing June–August for intensified ground monitoring, particularly around the Charlottetown–Summerside corridor. More broadly, pairing air-quality monitoring with energy-system planning—as in hybrid wind-battery design for remote communities like Nain, Newfoundland and Labrador [58]—may offer a complementary strategy for island and northern jurisdictions such as PE. In MA, the recurrent cold-season NO_2 maximum supports prioritizing December–February for enhanced ground monitoring along Greater Boston urban and transportation corridors. For CO, the strong temporal coherence between the jurisdictions and episodic enhancements support regional-background and smoke-event screening rather than compliance assessment. These recommendations identify when and where additional observations may be most informative; they do not establish source-specific controls, exposure thresholds, or regulatory interventions. An elevated satellite column should therefore be interpreted as a screening signal rather than as evidence that a surface air-quality standard has been exceeded. Decisions concerning emissions, human exposure, source attribution, or compliance require additional surface observations and, where appropriate, meteorological, source-apportionment, trajectory, exposure, or chemical-transport analyses. The direct policy contribution of this study is therefore a season- and

location-specific monitoring-prioritization framework rather than a prescriptive air-quality governance strategy.

4.2. Operational Monitoring Framework

The monitoring implications can be operationalized through the screening-to-follow-up framework summarized in Figure 9. Sentinel-5P first serves as a broad-area screening layer for identifying seasonally or spatially elevated column signals that may warrant closer investigation. In PE, the principal NO_2 signal is the warm-season enhancement, while in MA the recurrent cold-season pattern highlights urban and transportation corridors for winter-focused follow-up. Regional CO anomalies in either jurisdiction can similarly be used to flag candidate smoke or background-pollution episodes. These satellite-identified signals are then translated into candidate monitoring priorities rather than regulatory conclusions. Targeted follow-up can then be tailored to the jurisdiction-specific satellite signal. In PE, a practical strategy would combine intensified June–August reference-site observations with repeated daytime mobile transects or supplementary calibrated low-cost NO_2 sensors along the Charlottetown–Summerside corridor, with increased sampling during satellite-identified high-column episodes. In MA, winter follow-up could emphasize fixed or mobile measurements near major traffic and port-related corridors in Greater Boston, particularly during satellite-identified high-column episodes and shallow-mixing conditions. Supporting evidence from meteorology, air-mass trajectories, and emissions or source information can then be used to assess the context of the observed enhancements. Sentinel-5P therefore informs where and when additional monitoring may be most informative, whereas the final siting and operation of regulatory monitors remain governed by validated ground-network requirements.

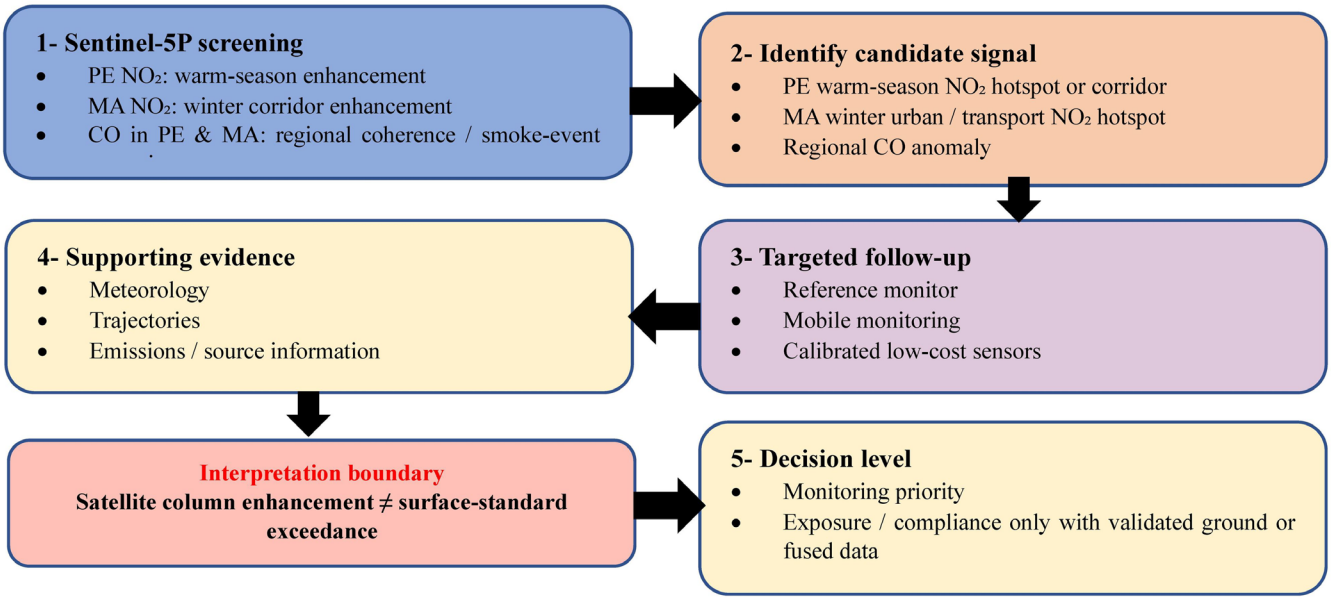


Figure 9. Screening-to-follow-up framework for translating Sentinel-5P column observations into monitoring priorities. Satellite screening is used to identify candidate seasonal or spatial signals, followed by targeted ground-based monitoring and supporting meteorological, trajectory, and source information. The framework supports monitoring prioritization, whereas exposure or regulatory-compliance assessment requires validated ground-based or appropriately fused evidence. Satellite column enhancement alone does not indicate surface-standard exceedance, and column burden is not interchangeable with surface concentration or local emission flux.

Within this framework, Sentinel-5P provides the spatially extensive screening capability needed to prioritize where and when more intensive observations may be most informative, while validated ground-based measurements provide the evidence required for exposure and compliance assessment. This screening-oriented role is consistent with recent applications of Sentinel-5P to environmental planning and air-quality resilience in sparsely monitored northern jurisdictions such as Yukon and Alaska [59]. A parallel Sentinel-5P framework for methane over Australia similarly combined satellite-based mapping with spatial clustering (Jenks–LISA, Global Moran's I) to identify persistent enhancement zones and translate them into priority-area screening for follow-up monitoring [60]. Satellite observations can therefore support more targeted allocation of monitoring resources without assuming that atmospheric column burden is equivalent to surface concentration or local emission flux. Where source attribution is required, supporting meteorological and trajectory information, and, where warranted, formal source-apportionment or chemical-transport modelling, should be incorporated before causal conclusions are drawn. Transparent documentation of retrieval-quality screening, temporal-completeness criteria, spatial processing, and analytical versions further supports reproducibility and subsequent validation of the framework.

5. Conclusions

This study investigates how multi-year, dual-pollutant satellite monitoring can clarify jurisdiction-scale air-quality dynamics in coastal and island environments. Integrating Sentinel-5P observations with surface indicators, we provide a coordinated assessment of CO and NO_2 across Prince Edward Island (PE) and Massachusetts (MA) from 2019 to 2024, contrasting a low-emission island with a densely urbanized coastal state under shared westerly circulation. The findings support the proposed hypotheses: H1 is confirmed, with PE and MA exhibiting closely similar CO means (≈0.0346 vs. 0.0348 mol m^{-2}, overlapping 95% CIs) and synchronous temporal anomalies, consistent with a strong regional-background influence. H2 is supported and refined, with the PE warm-season NO_2 enhancement identified as an emergent finding: NO_2 showed stronger jurisdiction-specific seasonality than CO, with MA winter maxima versus PE's pronounced warm-season peak (summer ≈ 7.5×10^{-5} vs. winter ≈ 3.9×10^{-5} mol m^{-2}), producing PE > MA contrasts outside winter. H3 is qualitatively supported: MA

exhibited compact localized NO_2 maxima along urban and transportation corridors, whereas PE showed a comparatively diffuse spatial pattern; this contrast is consistent with, but does not by itself explain, the higher PE jurisdiction-scale mean. H4 is qualitatively supported as a measurement-domain hypothesis: annual Sentinel-5P columns showed limited and construct-dependent concordance with independent evidence streams. The PE comparisons relate atmospheric column burden to reported emission flux, whereas the MA comparisons relate column burden to near-surface concentrations; these relationships are therefore interpreted separately rather than as jurisdiction-to-jurisdiction performance comparisons. Collectively, these findings are consistent with the proposed roles of pollutant lifetime, seasonal transport, source geometry, and satellite representativeness, though they do not independently establish causal attribution.

Several scoped limitations remain. Satellite columns represent vertically integrated quantities, not emissions or surface exposure; correspondence analysis is further limited to four annual paired observations per pollutant–jurisdiction comparison (five when the 2019 observation was included as a sensitivity check; Section 3.5). Steep urban gradients relative to pixel size and single-overpass timing introduce representativeness and temporal-mismatch errors. Strict filters, area-weighted means, and map classification may damp within-city heterogeneity and population-exposure contrasts. Mechanism testing is inferential: we do not embed chemical-transport modelling, apply systematic deweathering across all diagnostics, or perform formal source apportionment, and wildfire attribution is diagnostic rather than dynamically constrained. These caveats motivate a clear research agenda: (i) bias-aware fusion of columns with deweathered ground networks; (ii) stratification by weekday/weekend, heating season, and boundary-layer regime; (iii) transport diagnostics via back-trajectories, plume-height retrievals, and CTM experiments; (iv) corridor-scale monitoring and population-weighted exposure estimation; and (v) extension to additional coastal regions and interacting pollutants (e.g., O_3, PM) to test generalizability and health relevance.

Practical implications are intentionally limited to monitoring prioritization. Sentinel-5P columns should remain screening tools, while exposure assessment and compliance determinations require validated surface observations or fused products. PE's persistent warm-season NO_2 enhancement supports prioritizing summer ground monitoring around the Charlottetown–Summerside corridor, whereas MA's recurrent winter maximum supports enhanced winter monitoring along Greater Boston corridors. CO columns are most appropriately used for regional-background and smoke-event screening. These findings provide a transferable approach for identifying candidate monitoring periods and locations in coastal jurisdictions, while source-specific controls and broader governance interventions require additional meteorological, source-apportionment, exposure, and transport analyses.

Supplementary Materials: Table S1. Monthly trends of (a) CO and (b) NO_2 for Prince Edward Island and Massachusetts from January 2019 to December 2024. Table S2. Monthly column density of pollutants in the province of Prince Edward Island and the State of Massachusetts. Table S3. Average annual column density of pollutants in the province of Prince Edward Island and the State of Massachusetts. Table S4. Seasonal column density of pollutants in the province of Prince Edward Island and the State of Massachusetts.

Funding: This research received no external funding.

Author Contributions: Andrew d'Entremont: Investigation, Visualization, Writing—original draft. Akua Attoh: Investigation, Writing—review & editing. Amir Ghahremanlou: Investigation, Methodology, Conceptualization, Software, Writing—original draft. Davoud Ghahremanlou: Investigation, Conceptualization, Writing—review & editing. All authors have read and approved the final manuscript, and agreed to its publication in this journal.

Ethics approval: Not applicable.

Informed Consent Statement: Not applicable.

Data Availability Statement: Available from the corresponding author on reasonable request.

Declaration of Generative AI and AI-Assisted Technologies: During the preparation of this work, the authors used DeepSeek to improve readability and ChatGPT to assist in creating schematic figure elements. The authors reviewed and edited the content as needed and take full responsibility for the content of the manuscript.

Conflict of Interest: The authors declare that they have no conflict of interest.

References

[1] Allan, H.; Levin, N.; Kark, S. Quantifying and mapping the human footprint across Earth's coastal areas. *Ocean Coast. Manag.* **2023**, *236*, 106476. doi:10.1016/j.ocecoaman.2023.106476.

[2] Beyer, A.; Matthies, M. Long-Range transport potential of semivolatile organic chemicals in coupled air-water systems. *Environ. Sci. Pollut. Res.* **2001**, *8*(3), 173–179. doi:10.1007/BF02987382.

[3] Ghahremanlou, A.; Saffarzadeh, M.; Naderan, A.; Javanshir, H. Investigating the impact of accessibility on land use and its role in environmental pollution in Tehran. *Int. J. Transp. Eng.* **2022**, *9*(4), 833–854.

[4] Ghahremanlou, A.; Saffarzadeh, M.; Naderan, A.; Javanshir, H. Mechanism of the Effect of Urban Form and Land Use on Transportation and Air Pollution in Tehran. *Mon. Sci. J. Bagh-e Nazar* **2022**, *19*(109), 35–46. doi:10.22034/bagh.2022.323127.5086.

[5] Modak, A.K.; Bari, S.M.S.; Kamrul Islam, M.; Hossain, M.S. Spatiotemporal trends in columnar atmospheric pollutants around Hazrat Shahjalal International Airport using satellite remote sensing. *Int. J. Remote Sens.* **2026**, *47*(19), 8925–8955. doi:10.1080/01431161.2025.2589945.

[6] Liang, M.; Li, S.; Liang, Y.; Chen, M.; Song, Y.; Lu, Y.; et al. Toward an integrated governance framework for emerging contaminants. *Eco-Environ. Health* **2026**, *5*(2), 100239. doi:10.1016/j.eehl.2026.100239.

[7] Soni, M.; Arunachalam, S.; Ramarao, M.V.S.; Efstathiou, C.I.; Rick, C.; Buckley, L.; et al. A high resolution multipollutant assessment of health damages due to the onroad sector in Boston, Massachusetts. *Sci. Total Environ.* **2025**, *969*, 178847. doi:10.1016/j.scitotenv.2025.178847.

[8] Huang, M.; Carmichael, G.R.; Bowman, K.W.; De Smedt, I.; Colliander, A.; Cosh, M.H.; et al. Reactive nitrogen in and around the northeastern and mid-Atlantic US: sources, sinks, and connections with ozone. *Atmos. Chem. Phys.* **2025**, *25*, 1449–1476. doi:10.5194/acp-25-1449-2025.

[9] Bakola, M.; Hernandez Carballo, I.; Jelastopulu, E.; Stuckler, D. The impact of COVID-19 lockdown on air pollution in Europe and North America: A systematic review. *Eur. J. Public Health* **2022**, *32*(6), 962–968. doi:10.1093/eurpub/ckac118.

[10] Chen, H.; Zhang, W.; Sheng, L. Canadian record-breaking wildfires in 2023 and their impact on US air quality. *Atmos. Environ.* **2025**, *342*, 120941. doi:10.1016/j.atmosenv.2024.120941.

[11] Ehret, A.; Turquety, S.; George, M.; Hadji-Lazaro, J.; Clerbaux,

C. Increase in carbon monoxide (CO) and aerosol optical depth (AOD) observed by satellites in the Northern Hemisphere over the summers of 2008-2023, linked to an increase in wildfires. *Atmos. Chem. Phys.* **2025**, *25*(12), 6365–6394. doi:10.5194/acp-25-6365-2025.

[12] Borsdorff, T.; Campos, T.; Kille, N.; Zarzana, K.J.; Volkamer, R.; Landgraf, J. Vertical information of CO from TROPOMI total column measurements in context of the CAMS-IFS data assimilation scheme. *Atmos. Meas. Tech.* **2023**, *16*(11), 3027–3038. doi:10.5194/amt-16-3027-2023.

[13] Karppinen, T.; Sundström, A.-M.; Lindqvist, H.; Hatakka, J.; Tamminen, J. Satellite-based assessment of national carbon monoxide concentrations for air quality reporting in Finland. *Remote Sens. Appl. Soc. Environ.* **2024**, *33*, 101120. doi:10.1016/j.rsase.2023.101120.

[14] Marey, H.S.; Hashisho, Z.; Fu, L.; Gille, J. Spatial and temporal variation in CO over Alberta using measurements from satellites, aircraft, and ground stations. *Atmos. Chem. Phys.* **2015**, *15*(7), 3893–3908. doi:10.5194/acp-15-3893-2015.

[15] Goldberg, D.L.; Harkey, M.; de Foy, B.; Judd, L.; Johnson, J.; Yarwood, G.; et al. Evaluating NO_x emissions and their effect on O_3 production in Texas using TROPOMI NO_2 and HCHO. *Atmos. Chem. Phys.* **2022**, *22*(16), 10875–10900. doi:10.5194/acp-22-10875-2022.

[16] Tzortziou, M.; Kwong, C.F.; Goldberg, D.; Schiferl, L.; Commane, R.; Abuhassan, N.; et al. Declines and peaks in NO_2 pollution during the multiple waves of the COVID-19 pandemic in the New York metropolitan area. *Atmos. Chem. Phys.* **2022**, *22*(4), 2399–2417. doi:10.5194/acp-22-2399-2022.

[17] Van Geffen, J.; Eskes, H.; Compernolle, S.; Pinardi, G.; Verhoelst, T.; Lambert, J.-C.; et al. Sentinel-5P TROPOMI NO_2 retrieval: Impact of version v2.2 improvements and comparisons with OMI and ground-based data. *Atmos. Meas. Tech.* **2022**, *15*(7), 2037–2060. doi:10.5194/amt-15-2037-2022.

[18] Raifman, M.; Russell, A.G.; Skipper, T.N.; Kinney, P.L. Quantifying the health impacts of eliminating air pollution emissions in the City of Boston. *Environ. Res. Lett.* **2020**, *15*(9), 094017. doi:10.1088/1748-9326/ab842b.

[19] Drosoglou, T.; Bais, A.F.; Zyrichidou, I.; Kouremeti, N.; Poupkou, A.; Liora, N.; et al. Comparisons of ground-based tropospheric NO_2 MAX-DOAS measurements to satellite observations with the aid of an air quality model over the Thessaloniki area, Greece. *Atmos. Chem. Phys.* **2017**, *17*(9), 5829–5849. doi:10.5194/acp-17-5829-2017.

[20] Behera, S.; Kannemadugu, H.B.S.; K.G., D.; Taori, A. Satellite-based monitoring of NO_2 concentrations over thermal power plants around Delhi and assessing their role in Delhi air pollution. *Int. J. Remote Sens.* **2026**, *47*(19), 8828–8853. doi:10.1080/01431161.2025.2559424.

[21] Lacey, S.; Yang, J.; Ghahremanlou, D.; Ghahremanlou, A. Climate–Industry interplay in coastal air quality: A comparative Sentinel-5P study of the North Atlantic and Gulf of Mexico. *Challenges Sustain.* **2026**, *14*(3), 571–587. doi:10.56578/cis140309.

[22] Buchholz, R.R.; Deeter, M.N.; Worden, H.M.; Gille, J.; Edwards, D.P.; Hannigan, J.W.; et al. Validation of MOPITT carbon monoxide using ground-based Fourier transform infrared spectrometer data from NDACC. *Atmos. Meas. Tech.* **2017**, *10*(5), 1927–1956. doi:10.5194/amt-10-1927-2017.

[23] Zhou, Y.; Mao, H.; Demerjian, K.; Hogrefe, C.; Liu, J. Regional and hemispheric influences on temporal variability in baseline carbon monoxide and ozone over the Northeast US. *Atmos. Environ.* **2017**, *164*, 309–324. doi:10.1016/j.atmosenv.2017.06.017.

[24] Adams, T.J.; Geddes, J.A.; Lind, E.S. New Insights Into the Role of Atmospheric Transport and Mixing on Column and Surface Concentrations of NO_2 at a Coastal Urban Site. *J. Geophys. Res. Atmos.* **2023**, *128*(12), e2022JD038237. doi:10.1029/2022JD038237.

[25] Zhao, X.; Fioletov, V.; Alwarda, R.; Su, Y.; Griffin, D.; Weaver, D.; et al. Tropospheric and Surface Nitrogen Dioxide Changes in the Greater Toronto Area during the First Two Years of the COVID-19 Pandemic. *Remote Sens.* **2022**, *14*(7), 1625. doi:10.3390/rs14071625.

[26] Bechle, M.J.; Millet, D.B.; Marshall, J.D. Remote sensing of exposure to NO_2: Satellite versus ground-based measurement in a large urban area. *Atmos. Environ.* **2013**, *69*, 345–353. doi:10.1016/j.atmosenv.2012.11.046.

[27] Ialongo, I.; Virta, H.; Eskes, H.; Hovila, J.; Douros, J. Comparison of TROPOMI/Sentinel-5 Precursor NO_2 observations with ground-based measurements in Helsinki. *Atmos. Meas. Tech.* **2020**, *13*(1), 205–218. doi:10.5194/amt-13-205-2020.

[28] Shafran-Nathan, R.; Levy, I.; Levin, N.; Broday, D.M. Ecological bias in environmental health studies: The problem of aggregation of multiple data sources. *Air Qual. Atmos. Health* **2017**, *10*(4), 411–420. doi:10.1007/s11869-016-0436-x.

[29] Government of Canada. Provinces/Territories, Cartographic Boundary File—2016 Census. 2016. Available Online: https://open.canada.ca/data/en/dataset/a883eb14-0c0e-45c4-b8c4-b54c4a819edb.

[30] Government of the United States. US Census Bureau, Geography Division. 2024. Available Online: https://www.census.gov/cgi-bin/geo/shapefiles/index.php?year=2024&layergroup=States+%28and+equivalent%29.

[31] Beltran Vargas, N. Urban Air Pollution and Climate Stressors: Exploring Nitrogen Dioxide Patterns and Heat Wave Impacts in Holyoke, MA. Master Thesis, University of Massachusetts Amherst, Amherst, MA, U.S., 2025. doi:10.7275/55870.

[32] Borrego, C.; Souto, J.A.; Monteiro, A.; Dios, M.; Rodríguez, A.; Ferreira, J.; et al. The role of transboundary air pollution over Galicia and North Portugal area. *Environ. Sci. Pollut. Res.* **2013**, *20*(5), 2924–2936. doi:10.1007/s11356-012-1201-9.

[33] Ryu, Y.-H.; Min, S.-K. Anthropogenic warming degrades spring air quality in Northeast Asia by enhancing atmospheric stability and transboundary transport. *npj Clim. Atmos. Sci.* **2024**, *7*(1), 50. doi:10.1038/s41612-024-00603-7.

[34] Rijsdijk, P.; Eskes, H.; Dingemans, A.; Boersma, K.F.; Sekiya, T.; Miyazaki, K.; et al. Quantifying uncertainties in satellite NO_2 superobservations for data assimilation and model evaluation. *Geosci. Model Dev.* **2025**, *18*(2), 483–509. doi:10.5194/gmd-18-483-2025.

[35] Geddes, J.A.; Murphy, J.G.; O'Brien, J.M.; Celarier, E.A. Biases in long-term NO_2 averages inferred from satellite observations due to cloud selection criteria. *Remote Sens. Environ.* **2012**, *124*, 210–216. doi:10.1016/j.rse.2012.05.008.

[36] Government of Canada. Air Pollutant and Black Carbon Emissions Inventories. 2025. Available Online: https://pollution-waste.canada.ca/air-emission-inventory/.

[37] United States Environmental Protection Agency. United States Environmental Protection Agency Annual Air Data. 2025. Available Online: https://aqs.epa.gov/aqsweb/airdata/download_files.html#Annual.

[38] Ghahremanlou, A.; Ghahremanlou, D. Managing methane concentrations in western Canada: Climate actions towards a net-zero target. *Int. J. Remote Sens.* **2025**, *46*(23), 9330–9348. doi:10.1080/01431161.2025.2580780.

[39] Ghahremanlou, A.; Ghahremanlou, D. Identifying the Causes of Air Pollution in the Tehran Metropolis-Iran and Policy Recommendations for Sustainability. *Aerosol Sci. Eng.* **2026**, *10*, 370–384. doi:10.1007/s41810-025-00303-6.

[40] Fioletov, V.; McLinden, C.A.; Griffin, D.; Zhao, X.; Eskes, H.

Global seasonal urban, industrial, and background NO_2 estimated from TROPOMI satellite observations. *Atmos. Chem. Phys.* **2025**, *25*, 575–596. doi:10.5194/acp-25-575-2025.

[41] Angevine, W.M.; Žagar, M.; Tjernström, M.; Senff, C.J.; White, A.B. Coastal boundary layer transport of urban pollution in New England. 2004, 831–837. Available Online: https://ams.confex.com/ams/pdfpapers/77839.pdf.

[42] Griffin, D.; Zhao, X.; McLinden, C.A.; Boersma, F.; Bourassa, A.; Dammers, E.; et al. High-Resolution Mapping of Nitrogen Dioxide With TROPOMI: First Results and Validation Over the Canadian Oil Sands. *Geophys. Res. Lett.* **2019**, *46*(2), 1049–1060. doi:10.1029/2018GL081095.

[43] Shabbir, Y.; Zhou, G.; Obaid-ur-Rehman; Shah, S.R.A.; Ishaq, R.A. Trans-boundary spatio-temporal analysis of Sentinel 5P tropospheric nitrogen dioxide and total carbon monoxide columns over Punjab and Haryana Regions with COVID-19 lockdown impact. *Environ. Monit. Assess.* **2024**, *196*(3), 291. doi:10.1007/s10661-024-12458-9.

[44] Sun, B.Z.; Dahlberg, S.E.; Wallace, M.; Vallarino, J.; Lee, J. X.; Rice, M.B.; et al. Ambient smoke exposure and indoor air quality in eastern Massachusetts during the 2023 wildfire season. *J. Air Waste Manag. Assoc.* **2024**, *74*(11), 820–827. doi:10.1080/10962247.2024.2409790.

[45] Wang, Y.; Faloona, I.C.; Houlton, B.Z. Satellite NO_2 trends reveal pervasive impacts of wildfire and soil emissions across California landscapes. *Environ. Res. Lett.* **2023**, *18*(9), 094032. doi:10.1088/1748-9326/acec5f.

[46] Cheng, F.; Sun, Q.; Zhang, J.; Liu, J.; Lü, W.; Shen, F.; et al. Nitrogen dioxide pollution in 346 Chinese cities: Spatiotemporal variations and natural drivers from multi-source remote sensing data. *PLoS ONE* **2025**, *20*(11), e0334535. doi:10.1371/journal.pone.0334535.

[47] Luo, B.; Xiao, C.; Luo, D.; Fu, Q.; Chen, D.; Zhang, Q.; et al. Atmospheric and oceanic drivers behind the 2023 Canadian wildfires. *Commun. Earth Environ.* **2025**, *6*(1), 446. doi:10.1038/s43247-025-02387-x.

[48] Ademu, L.O.; Gao, J.; Thompson, O.P.; Ademu, L.A. Impact of Short-Term Air Pollution on Respiratory Infections: A Time-Series Analysis of COVID-19 Cases in California during the 2020 Wildfire Season. *Int. J. Environ. Res. Public Health* **2022**, *19*(9), 5057. doi:10.3390/ijerph19095057.

[49] Byrne, B.; Liu, J.; Bowman, K.W.; Pascolini-Campbell, M.; Chatterjee, A.; Pandey, S.; et al. Carbon emissions from the 2023 Canadian wildfires. *Nature* **2024**, *633*(8031), 835–839. doi:10.1038/s41586-024-07878-z.

[50] Saim, A.A.; Aly, M.H. Big data analyses for determining the spatio-temporal trends of air pollution due to wildfires in California using Google Earth Engine. *Atmos. Pollut. Res.* **2024**, *15*(9), 102226. doi:10.1016/j.apr.2024.102226.

[51] Geng, G.; Zhang, Q.; Martin, R.V.; Lin, J.; Huo, H.; Zheng, B.; et al. Impact of spatial proxies on the representation of bottom-up emission inventories: A satellite-based analysis. *Atmos. Chem. Phys.* **2017**, *17*(6), 4131–4145. doi:10.5194/acp-17-4131-2017.

[52] Sharafi, S.; Farahani, M.D. Satellite-Based Assessment of Urban Air Pollution Dynamics in Arak City with Implications for Public Health Risk. *Water Air Soil Pollut.* **2026**, *237*(1), 15. doi:10.1007/s11270-025-08740-2.

[53] Ghahremanlou, A.; Ghahremanlou, D. Detailed analysis of air pollution in the Canadian prairie region: A step toward net-zero emission. *Sci. Total Environ.* **2025**, *963*, 178492. doi:10.1016/j.scitotenv.2025.178492.

[54] Chen, M.; Talbot, R.; Mao, H.; Sive, B.; Chen, J.; Griffin, R.J. Air mass classification in coastal New England and its relationship to meteorological conditions. *J. Geophys. Res. Atmos.* **2007**, *112*(D10), D10S05. doi:10.1029/2006JD007687.

[55] DeBell, L.J.; Talbot, R.W.; Dibb, J.E.; Munger, J.W.; Fischer, E. V.; Frolking, S.E. A major regional air pollution event in the northeastern United States caused by extensive forest fires in Quebec, Canada. *J. Geophys. Res. D Atmos.* **2004**, *109*(D19), D19305. doi:10.1029/2004JD004840.

[56] Hegarty, J.; Mao, H.; Talbot, R. Winter- and summertime continental influences on tropospheric O_3 and CO observed by TES over the western North Atlantic Ocean. *Atmos. Chem. Phys.* **2010**, *10*(8), 3723–3741. doi:10.5194/acp-10-3723-2010.

[57] Naderi, S.; Tian, X.; An, C. Assessment of mobility trends and transportation-related emissions in Canadian cities during the post-COVID-19 pandemic period. *Environ. Syst. Res.* **2025**, *14*(1), 3. doi:10.1186/s40068-025-00394-7.

[58] Kotian, S.; Ghahremanlou, D. Design for hybrid power system in Newfoundland and Labrador: A case study for Nain. *Eur. J. Electr. Eng. Comput. Sci.* **2024**, *8*(1), 1–5. doi:10.24018/ejece.2024.8.1.598.

[59] McCarthy, M.; Ghahremanlou, D.; Ghahremanlou, A. Sentinel-5P evidence for low-carbon energy planning and Arctic air-quality resilience in Yukon and Alaska. *Green Low-Carbon Econ.* **2026**, 1–17. doi:10.47852/bonviewGLCE62029684.

[60] Ghahremanlou, A.; Ghahremanlou, D.; Burrows, D. Continental-scale spatiotemporal assessment of atmospheric methane over Australia: Hotspot persistence and priority-area screening. *Atmos. Environ.* **2026**, *375*, 121992. doi:10.1016/j.atmosenv.2026.121992.



Copyright: © 2026 by the author(s). *Net Zero* published by CoSci Press. This is an open access publication under the Creative Commons Attribution 4.0 International License (CC BY 4.0).